Submitted to *International Journal of Vehicle Design*, November 2003.

ON THE DETERMINATION OF DRIVER REACH AND BARRIERS

by

Jingzhou Yang*[1], Karim Abdel-Malek[1] and Kyle Nebel[2]
[1]Virtual Soldier Research Center
Center for Computer-Aided Design
The University of Iowa
116 Engineering Research Facility
Iowa City, IA 52242-1000
Tel No: (319) 335-6053
Fax No: (319) 384-0542
www.digital-humans.org

[2]U.S. Army TACOM/RDECOM
AMSRD-TAR-NAC/157
6501 East 11 Mile Rd.
Warren, MI 48397-5000
Ph (586) 574-8809
Fax (586) 574-6280

E-mail: **jyang@engineering.uiowa.edu**

Original Submission: November 2003

* Author to whom all correspondence should be addressed

Report Documentation Page

Form Approved
OMB No. 0704-0188

1. REPORT DATE	2. REPORT TYPE	3. DATES COVERED
01 NOV 2003	**Technical Report**	**01-06-2003 to 28-10-2003**

4. TITLE AND SUBTITLE
ON THE DETERMINATION OF DRIVER REACH AND BARRIERS

5a. CONTRACT NUMBER
5b. GRANT NUMBER
5c. PROGRAM ELEMENT NUMBER

6. AUTHOR(S)
Jingzhou Yang; Karim Abdel-Malek; Kyle Nebel

5d. PROJECT NUMBER
5e. TASK NUMBER
5f. WORK UNIT NUMBER

7. PERFORMING ORGANIZATION NAME(S) AND ADDRESS(ES)
Virtual Soldier Research Center,Center for Computer-Aided Design,116 Engineering Research Facility,Iowa City,IA,52242-1000

8. PERFORMING ORGANIZATION REPORT NUMBER
; #13982

9. SPONSORING/MONITORING AGENCY NAME(S) AND ADDRESS(ES)
U.S. Army TARDEC, AMSRD-TAR-NAC/157, 6501 East Eleven Mile Rd, Warren, Mi, 48397-5000

10. SPONSOR/MONITOR'S ACRONYM(S)
TARDEC

11. SPONSOR/MONITOR'S REPORT NUMBER(S)
#13982

12. DISTRIBUTION/AVAILABILITY STATEMENT
Approved for public release; distribution unlimited

13. SUPPLEMENTARY NOTES
For International Journal of Vehicle Design, November 2003

14. ABSTRACT
Design and packaging of vehicle interiors and cockpits had become a science on itself, particularly in recent years where safety is paramount. Significant experimental efforts have been made to study driver reach and barriers as they have direct effect on performance and safety. This paper presents a rigorous formulation for addressing the reach envelope and barriers therein of a 3-point restrained driver and compares with a lap-restrained driver. The formulation is based on a kinematic model of the driver, which has the upper body and arm characterized as a 7 degree of freedom (DOF) for unrestrained and 4DOF for 3-point restrained. Those kinematic equations are further developed to address crossability analysis. Visualization of such barriers and their crossability results within the reach envelope provide significant insight into driver performance and reach zones.

15. SUBJECT TERMS
SAE, driver reach, ergonomics, workspace, vehicle interior design

16. SECURITY CLASSIFICATION OF:			17. LIMITATION OF ABSTRACT	18. NUMBER OF PAGES	19a. NAME OF RESPONSIBLE PERSON
a. REPORT	b. ABSTRACT	c. THIS PAGE			
unclassified	**unclassified**	**unclassified**	**Public Release**	**32**	

Abstract

Design and packaging of vehicle interiors and cockpits had become a science on itself, particularly in recent years where safety is paramount. Significant experimental efforts have been made to study driver reach and barriers as they have direct effect on performance and safety. This paper presents a rigorous formulation for addressing the reach envelope and barriers therein of a 3-point restrained driver and compares with a lap-restrained driver. The formulation is based on a kinematic model of the driver, which has the upper body and arm characterized as a 7 degree of freedom (DOF) for unrestrained and 4DOF for 3-point restrained. Those kinematic equations are further developed to address crossability analysis. Visualization of such barriers and their crossability results within the reach envelope provide significant insight into driver performance and reach zones.

Keywords: SAE, driver reach, ergonomics, workspace, vehicle interior design

Introduction

Industrial tasks often involve repeated operator reach to various tools, parts and controls placed around a seated workstation. Examples include aircraft cockpit design, vehicle interior design and manufacturing workstations. All controls and other elements in the workstation requiring frequent manual operation should be placed in an area that focuses on optimizing the human interface for the target population, minimizing occlusion and reach, while providing maximum leverage for operation. The driver reach capability is a basis for developing a design aid in the form of reach contours that can be used easily by designers during the conceptual phase of a new vehicle program. While a database of reach barriers can be tabulated into a large database, we envision the implementation of the methodology into a digital human and simulation program such that reach barriers are calculated and visualized when needed during the design process.

The tool used for representing driver reach capabilities is the model developed in SAE Recommended Practice J287 by Hammond and Roe (1972). The SAE surfaces are parameterized by a packaging factor that combines vehicle interior dimensions such as seat height, fore-aft and vertical steering wheel position, and steering wheel diameter, into a single “G” score. This model is based on measurements taken of the actual reach capabilities of a representative sample of drivers and accounts for the design variation in workspace geometry of a wide range of vehicles in term of seat location, steering wheel position, and foot support. The test apparatus is shown in Figure 1 (adopted from Hammond and Roe 1972). Drivers were asked to grasp the ends of the measurement rods and to push forward as far as possible. The rod rack was moved laterally to span the

space in front of the driver. Testing was conducted with lap belt only and with lap and fixed-length torso belts. The data were analyzed to produce reach surfaces and Figure 2 depicts one such surface. Reach surfaces are interpreted with respect to population capability instead of the capability of individuals with particular body dimensions. 95 percent of drivers for a 50/50 male/female American driving population are expected to be able to reach to push-button targets that are located aft of the surface in Figure 2 instead of the reach capability of a male driver who is 95th percentile by stature.

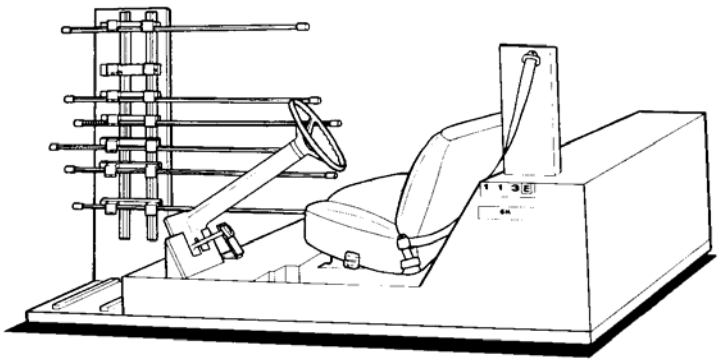

Figure 1 SAE control reach measuring fixture (Hammond and Roe 1972)

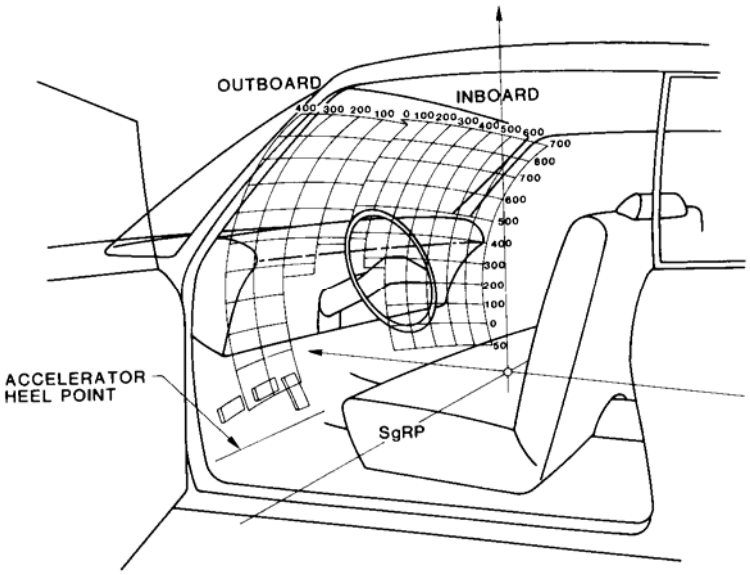

Figure 2 Control reach envelop in the vehicle workspace (Hammond and Roe 1972)

Digital human figure models have been used for the driver workstation assessments (Porter *et al.* 1993, 1995, and 1998; Chaffin 2001). Commercial digital human modeling and simulation programs are commonly used to simulate reach to controls with the outcomes of the digital human based studies used to assess control locations.

An experimental method was developed by Reed *et al*. (2003), which is based on a unified model of reach difficulty and capability. While experimented methods provide insight into the problem, extrapolating results to populations that have been used as subjects remains problematic. Furthermore, extracting mathematical models based on statistical data (typically non-linear regression) is particularly difficult. Parkinson *et al*. (2003) compared the reach envelope determined entirely by the segment lengths, joint degrees of freedom, and joint ranges of motion to those obtained in a laboratory study of men and women. Accurate prediction of maximum seated reach requires consideration of balance and pelvis mobility, neither of which is closely linked to joint range of motion. Sufficient ranges of motion in the shoulder and torso are also needed to represent postures near maximum reach.

In our previous work (Abdel-Malek *et al*. 2001a) we developed a method for understanding the workspace of upper extremities and Abdel-Malek *et al*. (2001b) developed a formulation for realistic posture prediction. For computation vehicle design systems, it is necessary to have analytical models to verify driver reach. Our ultimate goal is to enable the evaluation of driver discomfort for different positions of the controls within our analytical description of the reach envelope.

The understanding of trajectory formations inside the driver reach is, to a great extent, dependent upon the identification of control barriers that exist as impediments to motion and that may hinder the execution of a task. A rigorous mathematical formulation based on a kinematic model of the upper extremity will first be introduced. Because of this formulation, we will show that barriers inside the workspace are identified. More importantly, closed form equations of the workspace will be established. Furthermore, it will be shown that visualization of the internal of the workspace provides a powerful tool for barrier analysis. The analysis includes restrained reach of drivers, that is, drivers who are restrained by a non-extending shoulder belt and the unrestrained reach of drivers or drivers restrained by a lap belt only.

Modeling and Formulation

Whereas the anatomy of limbs and their joints are indeed very complex (as evidenced by the debate in the literature on the correct method for modeling joint motion), we will employ a kinematic pair (or combination thereof) as used in the field of robotics (which indicates a constrained kinematics joint). For example, if the resultant motion is rotational, the joint will be modeled as a revolute joint. The effect of a spherical joint is modeled as three revolute joints whose axes intersect at the center of the sphere. Indeed, all anatomical joints can be modeled using basic kinematic pairs.

Using *only four parameters* to describe one coordinate system with respect to another, the position and orientation of each axis determine the four parameters $\theta_i, d_i, a_i, \alpha_i$, and

hence, determine the resulting (4×4) transformation matrix. To establish this matrix, it is possible to observe that a vector ${}^{i}\mathbf{v}$ resolved in the *i*th coordinate system may be expressed in the (*i*-1)*th* coordinate system (${}^{i-1}\mathbf{v}$) by performing four successive transformations as follows.

(a) A rotation about the $\mathbf{z}_{i-1}$ axis by an angle of θ_i to align the $\mathbf{x}_{i-1}$ axis with the $\mathbf{x}_i$ axis (as shown in Figure 3, $\mathbf{x}_{i-1} // \mathbf{x}_i$ and pointing in the same direction).

(b) A translation along the $\mathbf{z}_{i-1}$ by a distance of d_i units to make $\mathbf{x}_{i-1}$ and $\mathbf{x}_i$ aligned.

(c) A translation along the $\mathbf{x}_i$ axis by a distance of a_i units to make the two origins of the i and $(i-1)$ systems coincide (the $\mathbf{x}_i$ and the $\mathbf{x}_{i-1}$ will also be aligned).

(d) A rotation about the $\mathbf{x}_i$ axis by an angle α_i to coincide the two coordinate systems.

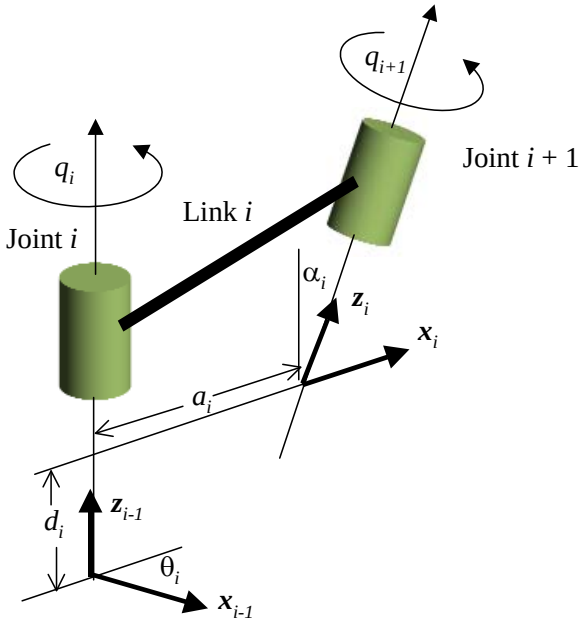

Figure 3 Establishing coordinate systems and the four D-H parameters

In order to obtain a systematic representation of any serial kinematic chain, we define $\mathbf{q} = [q_1 \quad ... \quad q_n]^T \in \mathbf{R}^n$ as the vector of *n*-generalized coordinates defining the motion of a limb with respect to another, where q_i is the individual DOF variable. The position

vector function (shown in Figure 4) generated by a point of interest (typically on one of the fingers) is written as a multiplication of rotation matrices and position vectors as

$$\mathbf{x}(\mathbf{q}) = \begin{bmatrix} x(\mathbf{q}) \\ y(\mathbf{q}) \\ z(\mathbf{q}) \end{bmatrix} = \sum_{i=1}^{i=n} [\prod_{j=1}^{j=i-1} {}^{j-1}\mathbf{R}_j]^{i-1}\mathbf{p}_i = \mathbf{\Phi}(\mathbf{q}) \tag{1}$$

where both ${}^{i}\mathbf{p}_j$ and ${}^{i}\mathbf{R}_j$ are defined using the Denavit-Hartenberg (D-H) representation method (Denavit and Hartenberg 1955, Paul 1981, and Fu *et al.* 1987) such that

$${}^{i-1}\mathbf{R}_i = \begin{bmatrix} \cos q_i & -\cos\alpha_i \sin q_i & \sin\alpha_i \sin q_i \\ \sin q_i & \cos\alpha_i \cos q_i & -\sin\alpha_i \cos q_i \\ 0 & \sin\alpha_i & \cos\alpha_i \end{bmatrix} \tag{2a}$$

and ${}^{(i-1)}\mathbf{p}_i = [a_i \cos q_i \quad a_i \sin q_i \quad d_i]^T$ (2b)

where q_i is the joint angle from $\mathbf{x}_{i-1}$ axis to the $\mathbf{x}_i$ axis, d_i is the shortest distance between $\mathbf{x}_{i-1}$ and $\mathbf{x}_i$ axes, a_i is the offset distance between $\mathbf{z}_i$ and $\mathbf{z}_{i-1}$ axes, and α_i is the offset angle from $\mathbf{z}_{i-1}$ and $\mathbf{z}_i$ axes.

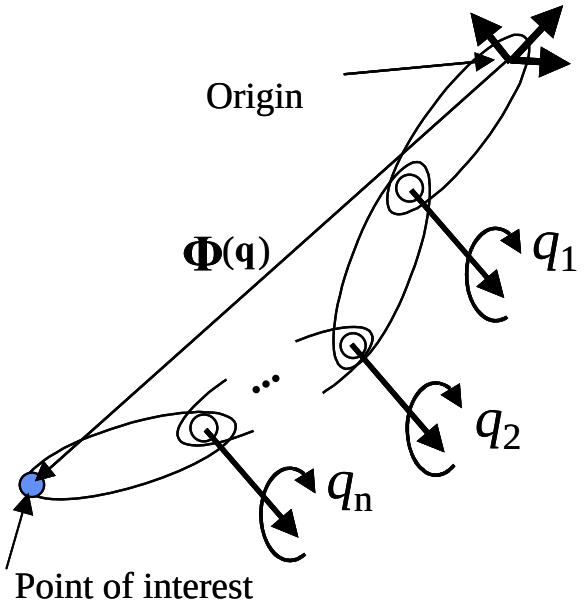

Figure 4 Definition of the position vector function $\mathbf{x}(\mathbf{q})$

The vector function $\mathbf{x}(\mathbf{q})$ characterizes the set of all points touched by the point of interest. The aim is to determine the envelope of this set. At a specified position in space given by (x_p, y_p, z_p), Eq. 1 can be written as a constraint function as

$$\begin{bmatrix} x(\mathbf{q}) - x_p \\ y(\mathbf{q}) - y_p \\ z(\mathbf{q}) - z_p \end{bmatrix} = \mathbf{0} \tag{3}$$

In mathematical terms, the expression defined by Eq. (3) is indeed a Manifold with boundary and cannot readily be visualized, because of the relatively large number of DOFs used to model the upper extremity.

Joint limits (ranges of motion) are imposed in terms of inequality constraints in the form of

$$q_i^L \le q_i \le q_i^U \tag{4}$$

where q_i^L and q_i^U are the lower and upper limits, respectively, and where $i = 1, \ldots n$, where *n* is the number of DOFs. Note that one joint could have more than one degrees of freedom (e.g., shoulder joint is modeled as three DOF). In order to include the range of motion in the formulation, we transform the inequalities above into equalities by introducing a new set of generalized coordinates $\boldsymbol{\lambda} = [\lambda_1 \quad \ldots \quad \lambda_n]^T$ such a joint variable is parameterized as

$$q_i = \tfrac{1}{2}(q_i^L + q_i^U) + \tfrac{1}{2}(q_i^U - q_i^L)\sin\lambda_i \qquad i = 1, \ldots, n \tag{5}$$

where if $\sin\lambda_i = 1$, then $q_i = q_i^U$ and when $\sin\lambda_i = -1$, then $q_i = q_i^L$. In order to include the effect of joint limits, it is proposed to augment the constraint equation with the parameterized inequality constraints of Eq. (5) such that

$$\mathbf{G}(\mathbf{q}) = \begin{bmatrix} x(\mathbf{q}) - x_p \\ y(\mathbf{q}) - y_p \\ z(\mathbf{q}) - z_p \\ q_i - (q_i^U + q_i^L)/2 - (q_i^U - q_i^L)/2 \sin \lambda_i \end{bmatrix} = \mathbf{0}, i = 1, \ \ldots \ n \tag{6}$$

where $\mathbf{q}^* = \begin{bmatrix} \mathbf{q}^T & \boldsymbol{\lambda}^T \end{bmatrix}^T$ is the vector of all generalized coordinates. Note that although $n-$ new variables (λ_i) have been added, $n-$ equations have also been added to the constraint vector function without loosing the dimensionality of the problem.

The *Jacobian* (named after the German Mathematician Carl G. Jacobi) of the constraint function $\mathbf{G}(\mathbf{q}^*)$ at a specific point $\mathbf{q}^0$ is the $(3+n) \times 2n$ matrix

$$\mathbf{G}_{\mathbf{q}^*} = \partial \mathbf{G} / \partial \mathbf{q}^* \tag{7}$$

where the subscript denotes a derivative. Note that the Jacobian is defined in mathematical terms as the derivative of the transformation (Taylor and Mann 1972) between **x** and **q**. With the modified formulation including joint limits, the Jacobian is expanded as

$$\mathbf{G}_{\mathbf{q}^*} = \left[\begin{array}{c|c} \mathbf{x}_\mathbf{q} & \mathbf{0} \\ \hline \mathbf{I} & \mathbf{q}_\boldsymbol{\lambda} \end{array} \right] \tag{8}$$

where $\mathbf{q}_\boldsymbol{\lambda} = \partial \mathbf{q} / \partial \boldsymbol{\lambda}$, $\mathbf{x}_\mathbf{q} = \partial \mathbf{x} / \partial \mathbf{q}$, $\mathbf{0}$ is a $(3 \times n)$ zero matrix, **I** is the identity matrix, and

$$\mathbf{x}_\mathbf{q} = \begin{bmatrix} x_{q_1} & x_{q_2} & \ldots & x_{q_n} \\ y_{q_1} & y_{q_2} & \ldots & y_{q_n} \\ z_{q_1} & z_{q_2} & \ldots & z_{q_n} \end{bmatrix} \tag{9}$$

$$\mathbf{q}_\boldsymbol{\lambda} = \begin{bmatrix} -((q_1^U - q_1^L)/2) \cos \lambda_1 & 0 & \ldots & 0 \\ 0 & -((q_2^U - q_2^L)/2) \cos \lambda_2 & \ldots & 0 \\ 0 & 0 & \ldots & 0 \\ 0 & 0 & \ldots & -((q_n^U - q_n^L)/2) \cos \lambda_n \end{bmatrix} \tag{10}$$

Because the Jacobian is not square (more than three DOFs), rank deficiency criteria were developed for surfaces that are swept in space (Abdel-Malek and Yeh 1997). These surfaces are called "barriers" provide significant insight towards better understanding reach and comfort within the workspace. Before addressing these criteria, however, it is important to show why the *singularity* of the Jacobian has a direct effect on identifying barriers and human reach. A singularity (in the pure mathematical sense) is when the Jacobian has no inverse, i.e., a solution cannot be found. To further explain, consider the differentiation of Eq. (1) with respect to time as

$$\dot{\mathbf{x}} = \mathbf{x}_{\mathbf{q}}\dot{\mathbf{q}} \tag{11}$$

where $\dot{\mathbf{q}}$ is the vector of joint velocities. Given the hand velocity (i.e., given $\dot{\mathbf{x}}$), the calculation of $\dot{\mathbf{q}}$ requires computing an inverse of the Jacobian $\mathbf{x}_{\mathbf{q}}$. For a singular Jacobian, it is not possible to compute the required velocities for such a path. It will be observed that such behavior is associated with barriers within the reach envelope (e.g., when the arm is fully extended and cannot extend any further, or when some joints in the arm have reached their limits).

We will use the idea of a singular Jacobian to identify all barriers inside and on the boundary of the workspace. Because the Jacobian is nonsquare, we define such barriers as a subset of the workspace at which the Jacobian of the constraint function of Eq. (7) is **row rank deficient**; i.e., barriers defined by a subset of the reach envelope ∂W and characterized by

$$\partial W \subset \left\{ \text{Rank } \mathbf{G}_{\mathbf{q}^*}(\mathbf{q}^*) < (n-2), \text{ for some } \mathbf{q}^* \text{ with } \mathbf{G}(\mathbf{q}^*) = \mathbf{0} \right\} \tag{12}$$

where k is at least $(3+n)$. Because of the form of the Jacobian characterized by Eq. (12), three distinct conditions arise:

(1) Type I singularity sets: If no joints have reached their limits, the diagonal sub-matrix $\mathbf{q}_\lambda$ is full row rank. Therefore, the only possibility for $\mathbf{G}_{\mathbf{q}^*}$ to be row-rank deficient is when the block matrix $\mathbf{x}_\mathbf{q}$ is row rank deficient. Type I singularity set is defined as

$$S^{(1)} \equiv \left\{ \mathbf{p} \in \mathbf{q} : \text{ Rank}[\mathbf{x}_\mathbf{q}] < 3, \text{ for some constant subset of } \mathbf{q} \right\} \tag{13}$$

where **p** is within the specified joint limit constraints and may contain joints that are functions of others or constant values.

(2) Type II singularity sets: When certain joints reach their limits, e.g., $\partial\mathbf{q}^{\lim} = [q_i^{\text{limit}}, q_j^{\text{limit}}, q_k^{\text{limit}}]^T$, the corresponding diagonal elements in the matrix $\mathbf{q}_\lambda$ will be equal to zero. Therefore, the corresponding matrix is subjected to the rank-deficiency criterion, where $\mathbf{G}_{\mathbf{q}^*}$ will take on the following form

$$\mathbf{G}_{\mathbf{q}^*} \sim \begin{bmatrix} \mathbf{x}_{q_1} & \dots & \mathbf{x}_{q_i} & \mathbf{x}_{q_j} & \mathbf{x}_{q_k} & \dots & \mathbf{x}_{q_n} \\ 0 & \dots & 1 & 0 & 0 & \dots & 0 \\ 0 & \dots & 0 & 1 & 0 & \dots & 0 \\ 0 & \dots & 0 & 0 & 1 & \dots & 0 \end{bmatrix} \tag{14}$$

and where the three columns pertaining to $\mathbf{x}_{q_i}$, $\mathbf{x}_{q_j}$, and $\mathbf{x}_{q_k}$ are removed such that the rank deficiency criteria are applied again. From the foregoing observation, the second type of singular sets are formulated. Define a new vector $\partial\mathbf{q}^{\text{limit}} = \left[q_i^{\text{limit}}, q_j^{\text{limit}}, q_k^{\text{limit}} \right]^T$, which is a sub-vector of $\mathbf{q}$ where $1 \le \dim(\partial\mathbf{q}^{\text{limit}}) \le (n-3)$.

The type II singularity set is defined as

$$S^{(2)} \equiv \left\{ \mathbf{p} = [\hat{\mathbf{p}} \cup \partial\mathbf{q}^{\text{limit}}] : \text{ Rank}[\mathbf{x}_\mathbf{q}(\mathbf{w}, \partial\mathbf{q}^{\text{limit}})] < 3, \text{for some } \hat{\mathbf{p}} \in \mathbf{q}, \ \mathbf{dim}(\partial\mathbf{q}^{\text{limit}}) \le (n-3) \right\}$$

(15)

where $\hat{\mathbf{p}}$ is the singular set as a result of applying the rank deficiency criteria to Eq. (14).

(3) Type III singularity sets: are all sets that are composed of the combination of joints at their limits and is defined by:

$$S^{(3)} = \{\mathbf{p} \in \mathbb{R}^{(n-2)} : \mathbf{p} = \mathbf{q}^{\text{limit}} \text{ for } [q_i^{\text{limit}}, q_j^{\text{limit}}, \ldots]; \text{ where } i \neq j \qquad (16)$$

Barriers are identified by substituting the sets $\mathbf{p}_i$ characterized by Eqs. (13, 15, and 16) into the accessible set $\mathbf{x}(\mathbf{q})$, which yields the equation of a surface that can be readily shown. This surface is indeed a barrier associated with a generalized variable that has reached its limit. Determining joint angles of the upper extremity given a specific position and orientation is usually defined as the inverse kinematics problem in the robotics literature (Fu, *et al*. 1987). Motion from one configuration to another along a trajectory sometimes requires halting the motion and changing the inverse kinematics in order to proceed with the motion. An example of this occurs when attempting to reach a point located behind one's shoulder. Starting with one trajectory may become very uncomfortable because of joint limits, while trying another trajectory becomes simpler and uninterrupted. Similarly, reaching a doorknob and turning sometimes is difficult to complete and requires orienting the initial hand configuration in a different posture. These barriers due to singular sets identified by Eqs. (13, 15, 16) may admit motion only in one normal direction, and hence are called impediments to motion.

Motion on a Barrier

To better understand when the hand may or may not cross barriers under given conditions, we explore the barrier's kinematic properties. We propose a criterion that is

based on normal acceleration at a point on a barrier, such that crossability is achieved if the barrier admits a normal acceleration in one direction or another. A point on a barrier admits motion normal to the surface in either direction depending on the difference in acceleration components (defined by the indicator η), such that

$$\eta = a_n - \frac{v_t^2}{\rho_o} \tag{17}$$

where v_t is the tangential velocity, a_n is normal acceleration, and $1/\rho_o$ is the normal curvature of the barrier *with respect to the tangent direction* of v_t (ρ_o is the radius of curvature). The need for formulating the problem in terms of velocities and accelerations will become apparent, as the resulting expression for the indicator η will be independent of acceleration values, but will be a quadratic form that has definiteness properties. A point on a singular surface will have no acceleration if the quantity η computes to null.

For a singular parametric entity $\mathbf{f}^{(i)}(\mathbf{u}^{(i)}) \in \mathbf{R}^3$ (where $\mathbf{u}$ is a vector representing the remaining joint variables—those not constant), and in the field of differential geometry, the *First Fundamental Form* (Farin 1993) is denoted by $\mathbf{I}_p$, where

$\mathbf{u}^{(i)} = \begin{bmatrix} u & v \end{bmatrix}^T = \begin{bmatrix} q_i & q_j \end{bmatrix}^T$, and is defined as

$$\mathbf{I}_p \equiv \delta\mathbf{u}^T \mathbf{f}_\mathbf{u}^T \mathbf{f}_\mathbf{u} \delta\mathbf{u} \tag{18}$$

where $\mathbf{f}_\mathbf{u} = \partial\mathbf{f}/\partial\mathbf{u}$. The *Second Fundamental Form* is defined as

$$\mathbf{II}_p \equiv \delta\mathbf{u}^T \left[\mathbf{N}^T \mathbf{f}\right]_{\mathbf{uu}} \delta\mathbf{u} \tag{19}$$

or expanded to

$$\mathbf{II}_p = \mathbf{N}^T \mathbf{f}_{uu} du^2 + 2\mathbf{N}^T \mathbf{f}_{uv} du\, dv + \mathbf{N}^T \mathbf{f}_{vv} dv^2 \tag{20}$$

where N is the vector normal to the singular surface and $\mathbf{f}_{uv} = \partial^2 \mathbf{f} / \partial u \partial v$. The Normal Curvature K_o of a parametric surface at a configuration $\mathbf{q}_o$, in the direction of du/dv, can then be defined as the ratio (Farin 1993)

$$K_o = \frac{1}{\rho_o} = \frac{\mathbf{II}_p}{\mathbf{I}_p} \tag{21}$$

In order to determine the kinematics quantities, we define the *Time-Modified First and Second Fundamental Forms* as

$$\mathbf{I}'_p \equiv \dot{\mathbf{u}}^T \mathbf{f}_\mathbf{u}^T \mathbf{f}_\mathbf{u} \dot{\mathbf{u}} \tag{22}$$

$$\mathbf{II}'_p \equiv \dot{\mathbf{u}}^T \left[\mathbf{N}^T \mathbf{f} \right]_{\mathbf{uu}} \dot{\mathbf{u}} \tag{23}$$

such that the normal curvature can still be defined as

$$K_o = \frac{1}{\rho_o} = \frac{\mathbf{II}_p}{\mathbf{I}_p} = \frac{\mathbf{II}'_p}{\mathbf{I}'_p} \tag{24}$$

For a singular surface $\mathbf{f}^{(i)}(\mathbf{u}^{(i)})$, the derivative using the chain rule is $\mathbf{f}_\mathbf{u} \dot{\mathbf{u}}$. Similarly, for the general singularity $\mathbf{\Phi}(\mathbf{q})$, the derivative is $\mathbf{\Phi}_\mathbf{q} \dot{\mathbf{q}}$. Therefore, at an instant of time, the tangential velocity in terms of $\mathbf{f}$ or $\mathbf{\Phi}$ at any point on the barrier is

$$\mathbf{v}_t = \mathbf{f}_\mathbf{u} \dot{\mathbf{u}} = \mathbf{\Phi}_\mathbf{q} \dot{\mathbf{q}} \tag{25}$$

If joint limits are considered, then the derivatives can be written as $\dot{\mathbf{u}} = \mathbf{u}_\lambda \dot{\boldsymbol{\lambda}}$ and $\dot{\mathbf{q}} = \mathbf{q}_\lambda \dot{\boldsymbol{\lambda}}$. The squared norm of the velocity is

$$\left| \mathbf{v}_t \right|^2 = \mathbf{v}_t^T \mathbf{v}_t = \dot{\mathbf{u}}^T \mathbf{f}_\mathbf{u}^T \mathbf{f}_\mathbf{u} \dot{\mathbf{u}} \tag{26}$$

which is equal to the Time-Modified First Fundamental Form $\mathbf{I}'_p$ of Eq. (22). Therefore, $\mathbf{I}'_p$ can be written as

$$\mathbf{I}'_p = \left| v_t \right|^2 \tag{27}$$

Substituting $1/\rho_o$ into η yields

$$\eta = a_n - \left| v_t \right|^2 \frac{\mathbf{II}'_p}{\mathbf{I}'_p} = a_n - \mathbf{II}'_p \tag{28}$$

When we consider Jacobian singular surfaces $a_n = \mathbf{N}^T \ddot{\mathbf{x}} = \dot{\mathbf{q}}^T \left[\mathbf{N}^T \mathbf{\Phi} \right]_{\mathbf{qq}} \dot{\mathbf{q}}$. Since a_n is in terms of $\dot{\mathbf{q}}$ and to express $\mathbf{II}'_p$ in terms of $\dot{\mathbf{q}}$, it was shown that the velocity vector on singular surface can be written as

$$\dot{\mathbf{u}} = \left[\mathbf{E} \mathbf{f}_{\mathbf{u}} \right]^{-1} \mathbf{E} \mathbf{\Phi}_{\mathbf{q}} \dot{\mathbf{q}} \tag{29}$$

where $E = \begin{bmatrix} 1 & 0 & 0 \\ 0 & 1 & 0 \end{bmatrix}$ if the first and second rows of $\mathbf{f}_{\mathbf{u}}$ are independent; $E = \begin{bmatrix} 1 & 0 & 0 \\ 0 & 0 & 1 \end{bmatrix}$ if the first and third rows of $\mathbf{f}_{\mathbf{u}}$ are independent; $E = \begin{bmatrix} 0 & 1 & 0 \\ 0 & 0 & 1 \end{bmatrix}$ if the second and third rows of $\mathbf{f}_{\mathbf{u}}$ are independent. Therefore the crossability criteria can be expanded into a quadratic form by

$$\eta = a_n - \mathbf{II}'_p = \dot{\mathbf{q}}^T \mathbf{Q} \dot{\mathbf{q}} \tag{30}$$

where

$$\mathbf{Q} = \left[\mathbf{N}^T \mathbf{\Phi} \right]_{\mathbf{qq}} - \mathbf{\Phi}_{\mathbf{q}}^T \mathbf{B} \left[\mathbf{N}^T \mathbf{f} \right]_{\mathbf{uu}} \mathbf{B} \mathbf{\Phi}_{\mathbf{q}} \tag{31}$$

and $\mathbf{B}$ is the generalized inverse of $\mathbf{f}_{\mathbf{u}}$ defined by

$$\mathbf{B} = \left[\mathbf{E} \mathbf{f}_{\mathbf{u}} \right]^{-1} \mathbf{E} \tag{32}$$

The matrix $\mathbf{Q}$ is calculated by substituting $\mathbf{q}_0$ into Eq.(31). The criteria is that if $\mathbf{Q}$ is indefinite, the interest point of the driver can admit normal movements along either direction of $\mathbf{N}$. The surface is crossable. If $\mathbf{Q}$ is semi-definite the surface is non-crossable.

When we consider the joint limits the component of the normal acceleration is then

$$a_n = \mathbf{N}^T \ddot{\mathbf{x}} = \dot{\boldsymbol{\lambda}}^T \mathbf{H}^* \dot{\boldsymbol{\lambda}} \tag{33}$$

where

$$\mathbf{H}^* = \dot{\mathbf{q}}_{\boldsymbol{\lambda}}^T \left[\mathbf{N}^T \boldsymbol{\Phi} \right]_{\mathbf{qq}} \dot{\mathbf{q}}_{\boldsymbol{\lambda}} + \sum_{i=1}^{n} \frac{d(\mathbf{N}^T \boldsymbol{\Phi})}{dq_i} \cdot \left[q_i \right]_{\boldsymbol{\lambda}\boldsymbol{\lambda}} \tag{34}$$

and the quadratic form is written in terms of the $\mathbf{Q}^*$ matrix as

$$\mathbf{Q}^* = \mathbf{H}^* - \mathbf{q}_{\boldsymbol{\lambda}}^T \boldsymbol{\Phi}_{\boldsymbol{\lambda}}^T \mathbf{B}^T \left[\mathbf{N}^T \mathbf{f} \right]_{\boldsymbol{\lambda}\boldsymbol{\lambda}} \mathbf{B} \boldsymbol{\Phi}_{\mathbf{q}} \mathbf{q}_{\boldsymbol{\lambda}} \tag{35}$$

If $\mathbf{Q}^*$ is indefinite the surface will definitely be crossable. However when $\mathbf{Q}^*$ is either positive semi-definite or negative semi-definite, the singular surface/curve may still be crossable. To address this case, we propose the projection of a variational movement $\delta \mathbf{x} = \mathbf{x}_{q_i} \delta q_i$ due to δq_i onto the normal direction $\mathbf{N}$ such that the normal component

$$\sigma = \mathbf{N}^T \mathbf{x}_{q_i} \delta q_i \tag{36}$$

determines admissible normal movement, where

$$\delta q_i = \begin{cases} +1 \; if \;\; q_i \; is \; at \; lower \; bound \\ -1 \;\; f \;\; q_i \; is \; at \; upper \; bound \end{cases} \tag{37}$$

Positive value of σ in Eq. (37) indicate the tip of the middle finger can admit movement in the positive direction of $\mathbf{N}$.

Another situation arises when the normal vector $\mathbf{N}$ is perpendicular to $\mathbf{x}_{q_i}$. In this case, σ evaluates to zero. Therefore we define the curvature difference

$$K_2 - K_1 = \frac{\delta q_i \left[\mathbf{N}^T \mathbf{x} \right]_{q_i q_i} \delta q_i}{\delta q_i \mathbf{x}_{q_i}^T \mathbf{x}_{q_i} \delta q_i} - \frac{\delta \mathbf{u}^T \left[\mathbf{N}^T \mathbf{f} \right]_{\mathbf{uu}} \delta \mathbf{u}}{\delta \mathbf{u} \mathbf{f}_{\mathbf{u}}^T \mathbf{f}_{\mathbf{u}} \delta \mathbf{u}} \tag{38}$$

We have

$$\delta \mathbf{u} = \mathbf{B}\mathbf{x}_{q_i}\delta q_i \tag{39}$$

Plugging Eq.(39) into Eq.(38) yields

$$K_2 - K_1 = \frac{\delta q_i \left[\mathbf{N}^T \mathbf{x}\right]_{q_i q_i} \delta q_i - \delta q_i \mathbf{x}_{q_i}^T \mathbf{B}^T \left[\mathbf{N}^T \mathbf{f}\right]_{\mathbf{uu}} \mathbf{B}\mathbf{x}_{q_i} \delta q_i}{\delta q_i \mathbf{x}_{q_i}^T \mathbf{x}_{q_i} \delta q_i} \tag{40}$$

The denominator of the right-hand side of Eq.(40) is always positive, the sign is dependent on the numerator. The numerator can be reduced to

$$\mu = K\delta q_i^2 \tag{41}$$

where

$$K = \mathbf{x}_{q_i}^T \mathbf{B}^T \left[\mathbf{N}^T \mathbf{x}\right]_{uu} \mathbf{B}\mathbf{x}_{q_i} - \left[\mathbf{N}^T \mathbf{x}\right]_{q_i q_i} \tag{42}$$

If $K > 0$, the tip of the middle finger can admit movement into the positive direction of $\mathbf{N}$. If $K < 0$, the tip of the middle finger can admit movement into the negative direction of $\mathbf{N}$. When $\mathbf{Q}^*$ is either positive semi-definite or negative semi-definite, The final criteria will be:

(1). If $\mathbf{N}$ is not perpendicular to $\mathbf{x}_{q_i}$, then σ in Eq.(36) must be evaluated.

(2). If $\mathbf{N}$ is perpendicular to $\mathbf{x}_{q_i}$, then K in Eq.(42) must be evaluated.

If any of σ or K has a different sign than the nonzero eigenvalues of $\mathbf{Q}^*$, the singular surface/curve is crossable; If σ and K have the same sign as nonzero eigenvalues of $\mathbf{Q}^*$, the singular surface/curve is non-crossable.

The Analysis of Restrained Drivers

Finding the Reach of Drivers

Consider the shoulder and forearm modeled as a 4-DOF system, where the spherical joint at the shoulder is modeled as three intersecting revolute joints and the elbow as a revolute joint. This is consistent with published results except that we have not considered the wrist joint (which is an additional 3 revolute joints) and we have limited the motion of the glenohumeral joint to spherical. It should be noted that this model does not include the scapulothoraic motion of the shoulder joint (i.e., the additional two translational DOFs of the scapulothoraic are not taken into consideration). Furthermore, we have modeled the spherical joint as three revolute joints intersecting at one point, a practice commonly made in modeling to represent spherical joints. It should be noted that the most difficult and the least successful modeling of a major articulating human joint has been the shoulder because of the difficulty in modeling the complex kinematic connectivities as well as the anatomical complexity of the region. Figure 5 depicts the joint motions to be modeled where each joint is given an independent coordinate q_i where the equivalent kinematic skeleton of the system is depicted with the z-axis located per the D-H representation method.

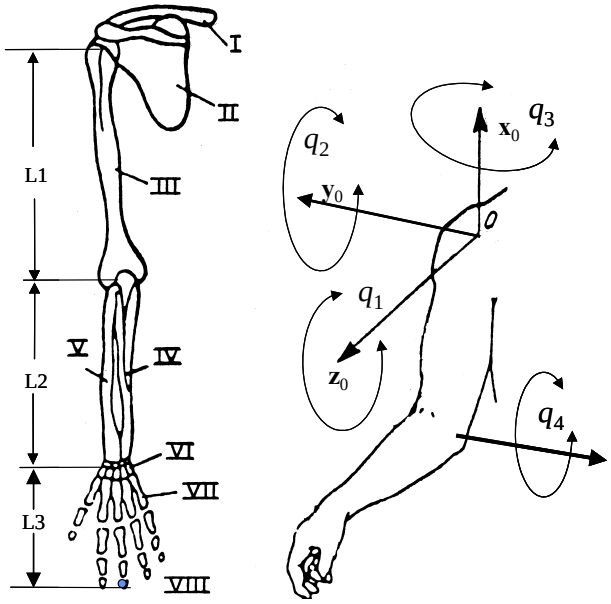

Figure 5 Shoulder and arm and the corresponding DOF

In the following analysis, a point on the tip of the middle finger as shown in Figure 6 will be tracked. The dimensions of the arm are different for different percentile humans. For 95^{th} percentile men the dimensions are $L1 = 40.64cm$, $L2 = 30.48cm$, $L3 = 20.32cm$, nevertheless, our method allows for any anthropometric data to be used in the formulation and is not percentile dependent. In the field of kinematics, the motion of a spherical joint with three DOFs can be modeled as three independent revolute joints having their axes intersecting at a single point as shown in Figure 6. Note that the point on the middle finger is shown located at the position ${}^4\mathbf{v} = [0 \quad 0 \quad 50.8]^T$ as resolved in the fourth coordinate frame.

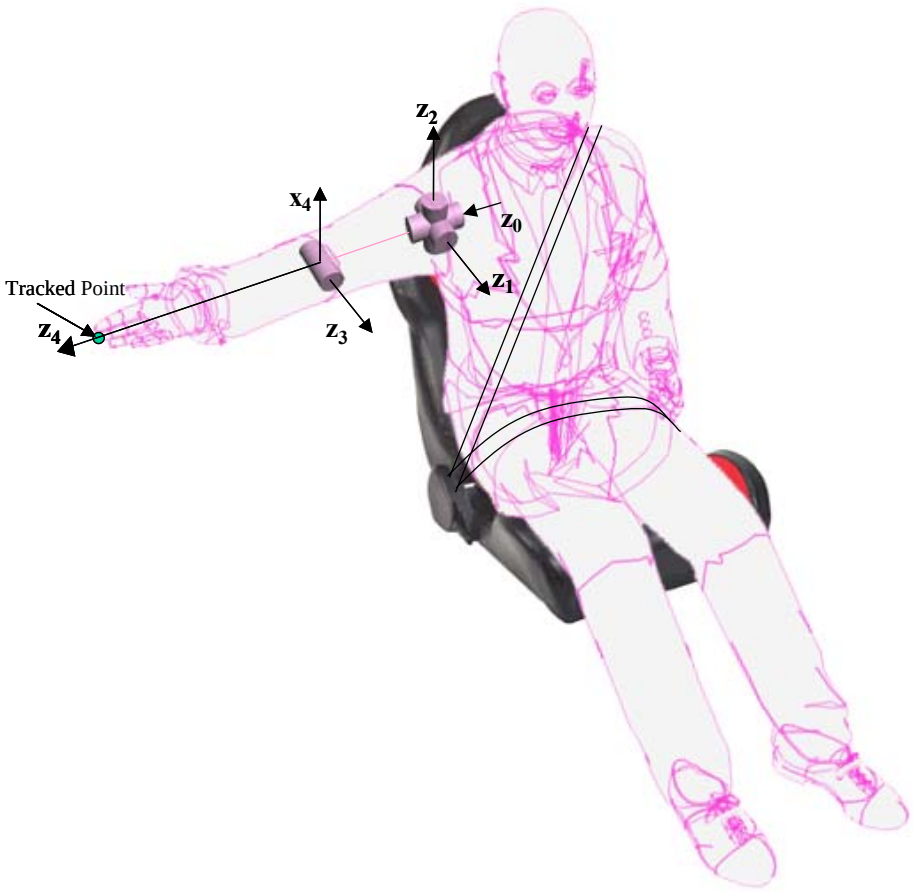

Figure 6 Kinematic modeling of the restrained driver

Consider the following joint limits imposed on the model of Fig. 6 for a 95th percentile male: $-90^o \le q1 \le 90$, $-110^o \le q2 \le 120^o$, $-90^o \le q3 \le 90^o$, and $-150^o \le q4 \le 0^o$. Using the Denavit-Hartenberg representation method, the position of the point of interest is given by Eq. (1) as

$$\mathbf{x}(\mathbf{q}) = \begin{bmatrix} (40.64 + 50.8\cos q_4)\sin q_1 \sin q_3 + \cos q_1(\cos q_3(-40.64 - 50.8\cos q_4)\sin q_2 - 50.8\cos q_2 \sin q_4) \\ \cos q_3(-40.64 - 50.8\cos q_4)\sin q_1 \sin q_2 + \cos q_1(-40.64 - 50.8\cos q_4)\sin q_3 - 50.8\cos q_2 \sin q_1 \sin q_4 \\ \cos q_2 \cos q_3(40.64 + 50.8\cos q_4) - 50.8\sin q_2 \sin q_4 \end{bmatrix} \tag{29}$$

Inequality constraints are parameterized as $q_1 = \pi/2 \sin\lambda_1$, $q_2 = \pi/36 + 23\pi/36 \sin\lambda_2$, $q_3 = \pi/2 \sin\lambda_3$, $q_4 = -5\pi/12 + 5\pi/12 \sin\lambda_4$. The rank deficiency criteria applied to the resulting (3◈4) Jacobian matrix yields 44 singular sets that are listed in Appendix A. Those singular sets are now substituted into Eq. (29), whereby parametric surface equations are readily plotted and visualized. For example several cross sections of the final driver reach envelope are shown in Figure 7.

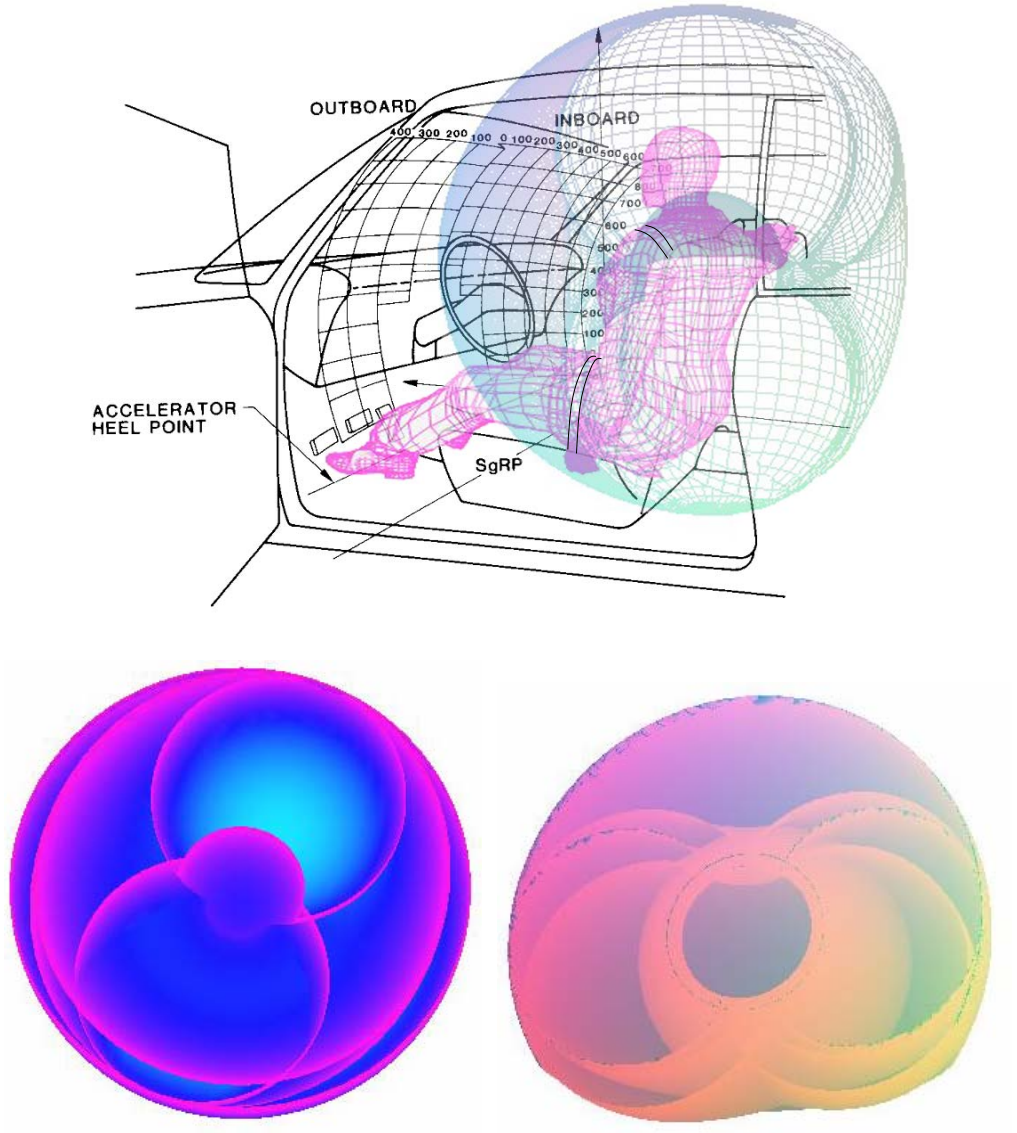

Figure 7. The cross sections of the restrained driver reach

Crossability Analysis of Singular Surfaces

A planer y_0oz_0 cross section view of the reach envelope at ($x_0 = 0$) is shown in Figure 8, where the intersection of the singular surfaces with plane traces curves that are called the singular curves and are denoted by Ψ_i, $i = 1,...,44$.

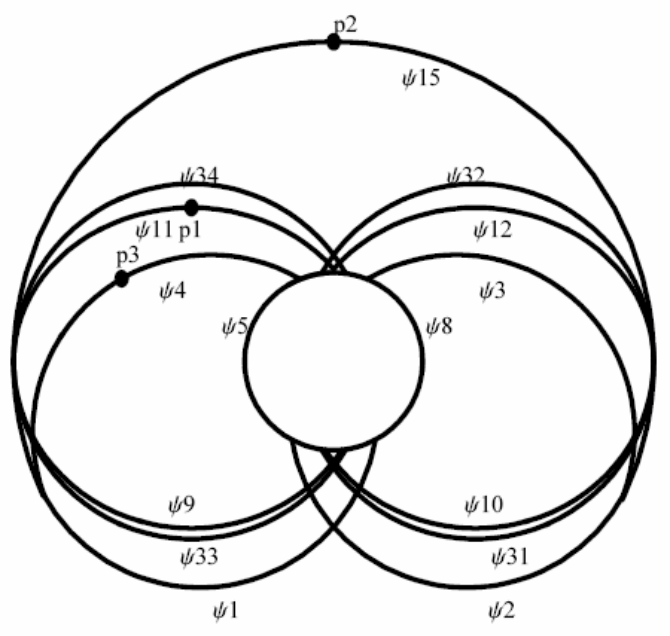

Figure 8 Cross Section of Singular surfaces

To demonstrate the crossability analysis, consider a point $\mathbf{p}_1$ on surface ψ_{11}, which has $\mathbf{q} = \begin{bmatrix} 0 & 2\pi/3 & \pi/2 & -\pi/2 \end{bmatrix}^T$ and $\boldsymbol{\lambda} = \begin{bmatrix} 0 & \pi/2 & \pi/2 & -\arcsin(1/5) \end{bmatrix}^T$. Evaluating the normal $\mathbf{N}$ from the basis of the null space of

$$\left[\boldsymbol{\Phi}_{\mathbf{q}} \mathbf{q}_{\lambda} \right]^T = \begin{bmatrix} 63.8372 & -39.8982 & 0 \\ 0 & 0 & 0 \\ 0 & 0 & 0 \\ 0 & -65.1535 & 0 \end{bmatrix}$$

at $\mathbf{p}_1$ yields the normal vector $\mathbf{N} = \begin{bmatrix} 0 & 0 & 1 \end{bmatrix}^T$. Evaluating the matrix $\mathbf{H}^*$ of Eq. (34) yields

$$\mathbf{H}^* = \begin{bmatrix} 0 & 0 & 0 & 0 \\ 0 & 50.9811 & 0 & 0 \\ 0 & 0 & -31.9186 & 0 \\ 0 & 0 & 0 & -72.3674 \end{bmatrix}$$

The singular surface is

$$\mathbf{f}(\mathbf{u}) = \begin{bmatrix} (40.64 + 50.8\cos q_4)\sin q_1 + 25.4\cos q_1 \sin q_4 & \cos q_1(-40.64 - 50.8\cos q_4) + 25.4\sin q_1 \sin q_4 & -43.9941\sin q_4 \end{bmatrix}^T$$

and its Jacobian matrix can be defined by

$$\mathbf{f}_\mathbf{u}(0, -\pi/2) = \begin{bmatrix} 40.64 & 0 \\ -25.4 & -50.8 \\ 0 & 0 \end{bmatrix}$$

Therefore the matrix $\mathbf{E}$ is

$$\mathbf{E} = \begin{bmatrix} 1 & 0 & 0 \\ 0 & 1 & 0 \end{bmatrix}$$

and

$$\mathbf{B} = \left[\mathbf{E}\mathbf{f}_\mathbf{u}\right]^{-1}\mathbf{E} = \begin{bmatrix} 0.0246063 & 0 & 0 \\ -0.0123031 & -0.019685 & 0 \end{bmatrix}$$

The matrix $\mathbf{Q}^*$ of the quadratic form is evaluated as

$$\mathbf{Q}^* = \begin{bmatrix} 0 & 0 & 0 & 0 \\ 0 & 50.9811 & 0 & 0 \\ 0 & 0 & -31.9186 & 0 \\ 0 & 0 & 0 & 0 \end{bmatrix}$$

The eigenvalues of $\mathbf{Q}^*$ are evaluated as $\begin{Bmatrix} 50.9811 & -31.9186 & 0 & 0 \end{Bmatrix}$, which indicates an indefinite quadratic form. Therefore it is a crossable surface at point $\mathbf{p}_1$. Crossability at this point means that a driver with a posture characterized by the singular set s_{11}, would allow the hand to cross that surface (represented by a singular curve). This is the first step towards better understanding comfort, dexterity, effort, and energy zones associated with driver reach.

To further demonstrate this, consider a point $\mathbf{p}_2$ on surface ψ_{15}, which has a configuration of $\mathbf{q} = \begin{bmatrix} -\pi/2 & 0 & 0 & 0 \end{bmatrix}^T$ and $\boldsymbol{\lambda} = \begin{bmatrix} -\pi/2 & \arcsin(-1/23) & 0 & \pi/2 \end{bmatrix}^T$. The normal vector at this point is calculated as $\mathbf{N} = \begin{bmatrix} 0 & 0 & 1 \end{bmatrix}^T$. The matrix $\mathbf{Q}$ is computed and its nonzero eigenvalue is -22.5778. Since $\mathbf{Q}$ is negative semi-definite, the singular surface ψ_{15} is non-crossable.

Consider a point $\mathbf{p}_3$ on surface ψ_4, which is a Jacobian singular surface and has a configuration $\mathbf{q} = \begin{bmatrix} \pi/2 & 2\pi/3 & 0 & -\pi/2 \end{bmatrix}^T$ and $\boldsymbol{\lambda} = \begin{bmatrix} \pi/2 & \pi/2 & 0 & -\arcsin(1/5) \end{bmatrix}^T$. The normal vector is $\mathbf{N} = \begin{bmatrix} 0 & -0.5 & 0.866025 \end{bmatrix}^T$. The nonzero eigenvalue of $\mathbf{Q}^*$ is obtained as 81.5697. Since the matrix is positive semi-definite, the supplementary criteria must be computed to ascertain crossability. For this surface, the joint variables q_1 and q_2 are at their limits. The variational normal movement of σ_n for δq_1 and δq_2 are also calculated as 0 and –40.64 respectively. For δq_1 the value of σ_n is 0 and we can calculate the Eq.(42) and $K = -30.2976$. The signs of σ_n for δq_2 and K for δq_1 are different from the sign of nonzero eigenvalue. Therefore, the surface ψ_4 at this point is crossable. Use the same procedure to check the points on other surfaces and the final admissible normal movement directions are shown in Figure 9.

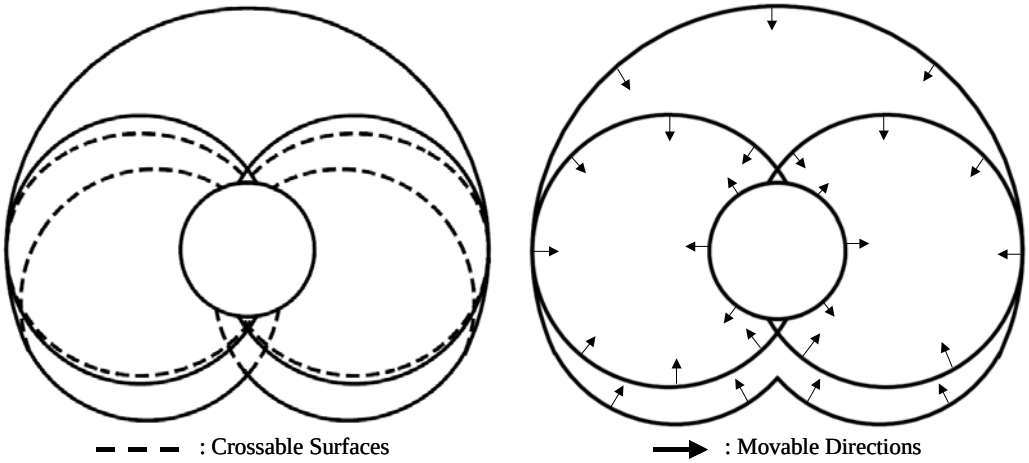

Figure 9 Crossable and non-crossable singular curves

The Unrestrained Reach of Drivers

Consider the upper body modeled as a 7-DOF system, where the upper extremity is the same as the restrained model in Figure 6. In order to account for the upper torso motion for an unrestrained driver, we propose the addition of 3 degrees of freedom representing motion at the waist. The torso part has three DOFs (spherical joints) and they are intersected into one point characterizing a seated driver with spherical articulation at the waist. Consider the following joint limits imposed on the model of Figure 10 for a 95th percentile male model: $-45^o \le q_1 \le 45^o$, $0^o \le q_2 \le 30^o$, $-30^o \le q_3 \le 30^o$, $-90^o \le q_4 \le 90^o$, $-110^o \le q_5 \le 120^o$, $-90^o \le q_6 \le 90^o$, and $-150^o \le q_7 \le 0^o$.

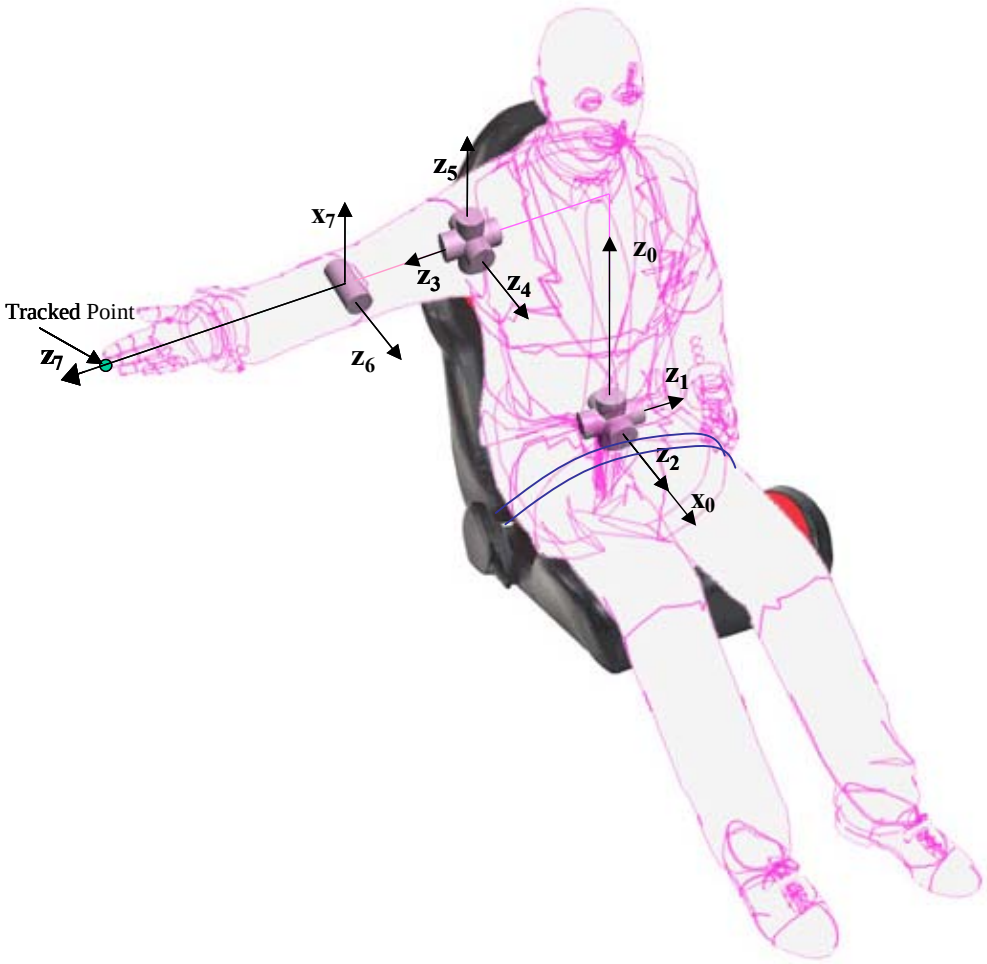

Figure 10. Kinematic modeling of the unrestrained driver

According to the D-H method, the tracked point of interest is

$$\begin{aligned}\mathbf{x}(\mathbf{q})[1] = {} & 25c_1c_3s_2 + 25s_1s_3 + 10c_3s_1 - 10c_1s_2s_3 + 16c_6(c_5(c_3s_1 - c_1s_2s_3) - (c_4(c_1c_3s_2 + s_1s_3) - c_1c_2s_4)s_5) + \\ & + 16(c_1c_2c_4 + (c_1c_3s_2 + s_1s_3)s_4s_6 + 20(c_7(c_6(c_5(c_3s_1 - c_1s_2s_3) - (c_4(c_1c_3s_2 + s_1s_3) - c_1c_2s_4)s_5) + \\ & (c_1c_2c_4 + (c_1c_3s_2 + s_1s_3)s_4)s_6) + (-c_5(c_4(c_1c_3s_2 + s_1s_3) - c_1c_2s_4) - (c_3s_1 - c_1s_2s_3)s_5)s_7)\end{aligned}$$

$$\begin{aligned}\mathbf{x}(\mathbf{q})[2] = {} & 25c_3s_1s_2 + 25s_1s_3 - c_1s_3 + 10(-c_1c_3 - s_1s_2s_3) + 16c_6(c_5(-c_1c_3 - s_1s_2s_3) - (c_4(c_3s_1s_2 - c_1s_3) \\ & - c_2s_1s_4)s_5) + 16(c_2c_4s_1 + (c_3s_1s_2 - c_1s_3s_4)s_6 + 20(c_7(c_6(c_5(-c_1c_3 - s_1s_2s_3) - (c_4(c_3s_1s_2 \\ & - c_1s_3) - c_2s_1s_4)s_5) + (c_2c_4s_1 + (c_3s_1s_2 - c_1s_3s_4)s_6) + (-c_5(c_4(c_3s_1s_2 - c_1s_3) - c_2s_1s_4) - \\ & (-c_1c_3 - s_1s_2s_3)s_5)s_7)\end{aligned}$$

$$\mathbf{x}(\mathbf{q})[3] = 25c_2c_3 - 10c_2s_3 + 16c_6(-c_2c_5s_3 - (c_2c_3c_4 + s_2s_4s_5) + 16(-c_4s_2 + c_2c_3s_4)s_6 + 20(c_7(c_6(-c_2c_5s_3$$
$$-(c_2c_3c_4 + s_2s_4s_5) + (-c_4s_2 + c_2c_3s_4)s_6) + (-c_5(c_2c_3c_4 + s_2s_4) + c_2s_3s_5)s_7)$$

Figure 11 shows the cross section of the unrestrained driver reach in the car. A x_0z_0 cross sectional plane showing the intersections of the singular surfaces with the plane as singular curves is shown in Figure 12.

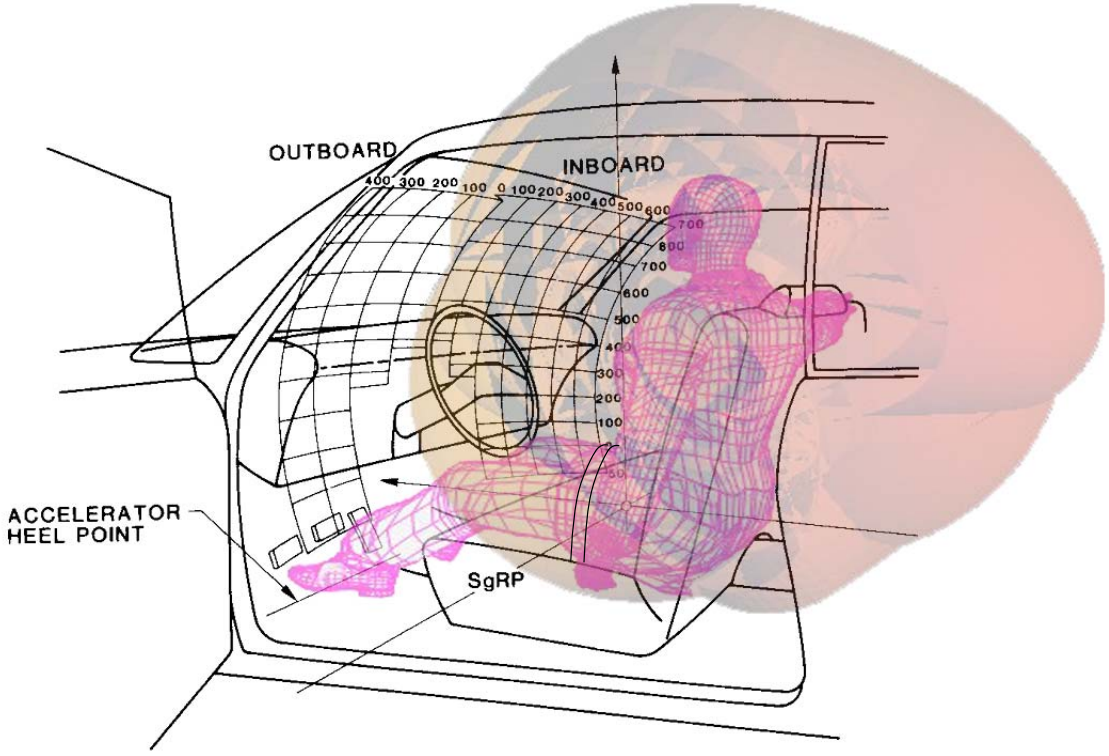

Figure 11. The cross section of the unrestrained driver reach ($y_0 = -10$)

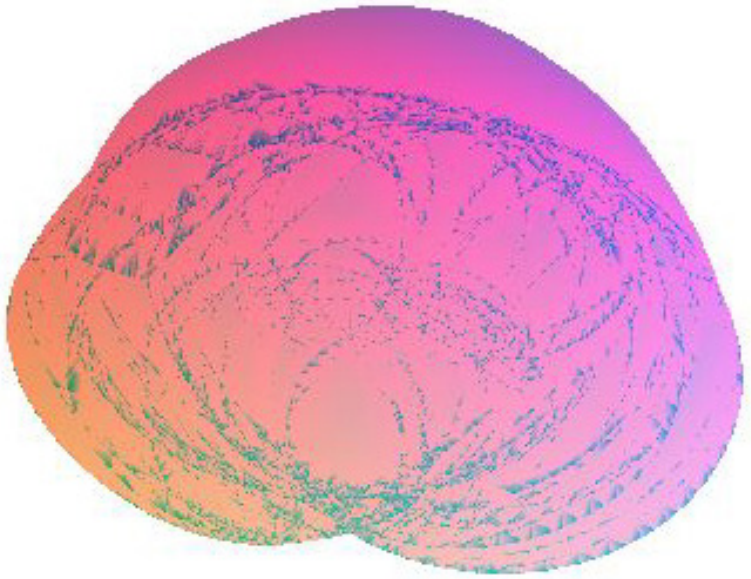

Figure 12. The cross section at $x_0 = 0$

We follow the procedure for determining the crossability of singular surfaces and obtain the crossabilities of the boundary surfaces of the unrestrained driver reach in Figure 13.

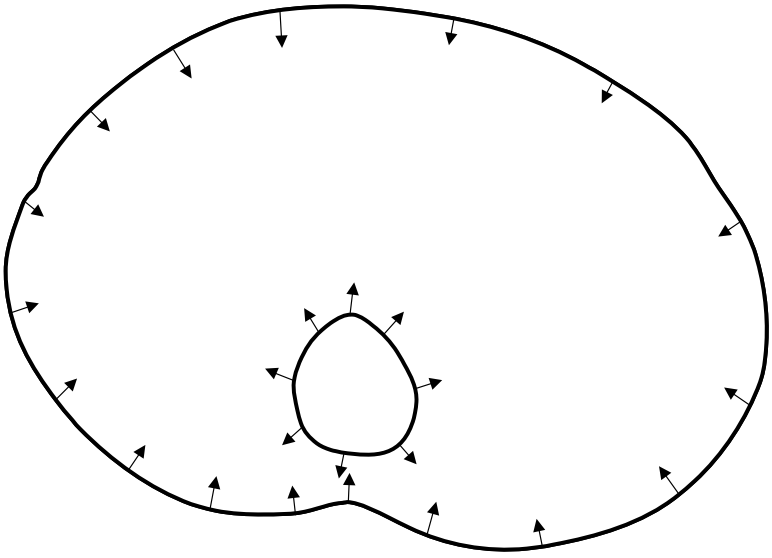

Figure 13. Boundary surfaces and their non-crossabilities ($x_0 = 0$)

Obviously, unrestrained driver reach gives rise to significantly more redundancy as there are significantly more singular curves. It is also observed that far more crossable surfaces in both directions are observed in the unrestrained case, as expected, because of the redundant 7 DOF model.

Conclusions

A formulation for visualizing restrained and unrestrained driver reach envelope has been presented, particularly the identification of singular surfaces within upon which Jacobian singularities occur. The work is aimed better understanding human-machine interaction from a human perspective, where the ultimate goal is to delineate regions and zones of common and quantifiable characteristics such as comfort, effort, energy, etc. This initial stage has focused on the understanding of barriers within the envelope upon which specific postures may or may not allow for crossability from kinematic point of view. It was shown that restrained drivers whose upper extremity is modeled as a 4DOF kinematic linkage has far more non-crossable (i.e. crossable surfaces in one direction at a particular singular configuration) than unrestrained drivers modeled as a 7DOF kinematic linkage. It was also shown that crossability at a singular curve within the reach envelope can now be determined in closed form and based as a first but necessary step towards delineating zones and regions within the envelope associated with driver quantifiable properties.

References

1. Abdel-Malek, K. and Yeh, H.J., 1997, "Geometric Representation of the Swept Volume Using Jacobian Rank-Deficiency Conditions," *Computer Aided Design*, Vol. 29, No. 6, pp. 457-468.

2. Abdel-Malek, K., Yang, J., Brand, R., Tanbour, E., (2001a), “Towards Understanding the workspace of the upper extremities,” *SAE Technical Paper* 2001-01-2095. (Also appears in *2001 SAE Transactions-Journal of Passenger Cars: Mechanical Systems*, Vol. 110, Section 6, pages 2198-2206).
3. Abdel-Malek, K., Yu, W., and Jaber, M., (2001b),"Realistic Posture Prediction", *Proceedings of 2001 SAE Digital Human Modeling for Design and Engineering*, June 26-28, Arlington, VA, USA.
4. Chaffin, D.B., Digital Human Modeling for Vehicle and Workspace Design, SAE International, Warrendable, PA, 2001.
5. Denavit, J. and Hartenberg, R.S., (1955), "A Kinematic Notation for Lower-Pair Mechanisms Based on Matrices", *Journal of Applied Mechanics*, vol.77, pp.215-221.
6. Farin, Gerald, Curves and Surfaces for CAGD, A Practical Guide, Academic Press, 1988.
7. Fu, K.S., Gonzalez, and Lee, C.S., 1987, *Robotics: Control, Sensing, Vision, And Intelligence*, McGraw-Hill, Inc., New York.
8. Hammond, D. C. and Roe, R. W., “SAE Controls Reach Study,” *SAE Technical paper* 720199.
9. Paul, R.P., 1981, *Robot Manipulators: Mathematics, programming, and Control*. MIT Press, Cambridge, Massachusetts.
10. Porter, J. M., Case, K., Freer, M. T., and Bonney, M. C., Computer-aided ergonomics design of automobiles. In Automotive Ergonomics, Ed. B. Peacock and W. Karwowski, 43-77. London: Taylor and Francis, 1993.
11. Porter, J.M., Freer, M., Case, K. and Bonney, M.C., 1995, “Computer Aided Ergonomics and Workspace Design,” *Evaluation of human Work : A Practical Ergonomics Methodology*, 2nd edition, Eds. Wilson, J.A. and Corlett, E.N., Taylor & Francis Ltd., pp 574-620.
12. Porter, J.M. and Porter, C.S., 1998, “Turning automotive design 'inside-out',” *International Journal of Vehicle Design,* Vol. 19, no 4, 385-401. ISSN 0143-3369.
13. Porter, J.M. and Gyi. D.E., 1998, “Exploring the optimum posture for driver comfort,” *International Journal of Vehicle Design*, Vol 19, no 3, 255-266. ISSN 0143-3369.
14. Parkinson, M.B., Reed, M.P., and Klinkenberger, A.L., "Assessing the validity of kinematically generated reach envelopes", *SAE Digital Human Modeling Conference*, 2003.
15. Reed, M. P., Parkinson, M., and Chaffin, D. B., “A New Approach to Modeling Driver Reach,” *SAE Technical Paper* 2003-01-0587.
16. Taylor A.E. and Mann, W.R. [1972]. *Advanced Calculus*, Xerox, Corp.

Appendix A

$s_1 = \{q_1 = -\pi/2, q_2 = -11\pi/18\}$, $s_2 = \{q_1 = \pi/2, q_2 = -11\pi/18\}$,

$s_3 = \{q_1 = -\pi/2, q_2 = 2\pi/3\}$, $s_4 = \{q_1 = \pi/2, q_2 = 2\pi/3\}$,

$s_5 = \{q_1 = -\pi/2, q_3 = -\pi/2\}$, $s_6 = \{q_1 = -\pi/2, q_3 = \pi/2\}$,

$s_7 = \{q_1 = \pi/2, q_3 = -\pi/2\}$, $s_8 = \{q_1 = \pi/2, q_3 = \pi/2\}$,

$s_9 = \{q_2 = -11\pi/18, q_3 = \pi/2\}$, $s_{10} = \{q_2 = -11\pi/18, q_3 = -\pi/2\}$,

$s_{11} = \{q_2 = 2\pi/3, q_3 = \pi/2\}$, $s_{12} = \{q_2 = 2\pi/3, q_3 = -\pi/2\}$

$s_{13} = \{q_1 = -\pi/2, q_4 = -5\pi/6\}$, $s_{14} = \{q_1 = \pi/2, q_4 = -5\pi/6\}$,

$s_{15} = \{q_1 = -\pi/2, q_4 = 0\}$, $s_{16} = \{q_1 = \pi/2, q_4 = 0\}$,

$s_{17} = \{q_2 = -11\pi/18, q_4 = -5\pi/6\}$, $s_{18} = \{q_2 = -11\pi/18, q_4 = 0\}$,

$s_{19} = \{q_2 = 2\pi/3, q_4 = -5\pi/6\}$, $s_{20} = \{q_2 = 2\pi/3, q_4 = 0\}$,

$s_{21} = \{q_3 = -\pi/2, q_4 = -5\pi/6\}$, $s_{22} = \{q_3 = \pi/2, q_2 = -5\pi/6\}$,

$s_{23} = \{q_3 = -\pi/2, q_4 = 0\}$, $s_{24} = \{q_3 = \pi/2, q_4 = 0\}$,

$s_{25} = \left\{q_1 = -\pi/2, q_4 = -Arc\cos(-\frac{4}{5})\right\}$, $s_{26} = \left\{q_1 = \pi/2, q_4 = -Arc\cos(-\frac{4}{5})\right\}$,

$s_{27} = \{q_2 = -11\pi/18, q_3 = 0\}$, $s_{28} = \{q_2 = 2\pi/3, q_3 = 0\}$,

$s_{29} = \left\{q_2 = 2\pi/3, q_4 = -Arc\cos(-\frac{4}{5})\right\}$, $s_{30} = \left\{q_2 = -11\pi/18, q_4 = -Arc\cos(-\frac{4}{5})\right\}$,

$s_{31} = \{q_3 = -\pi/2, q_2 = -\pi/2\}$, $s_{32} = \{q_3 = -\pi/2, q_2 = \pi/2\}$,

$s_{33} = \{q_3 = \pi/2, q_2 = -\pi/2\}$, $s_{34} = \{q_3 = \pi/2, q_2 = \pi/2\}$,

$s_{35} = \{q_2 = 0, q_4 = -5\pi/6\}$, $s_{36} = \{q_2 = 0, q_4 = -5\pi/6\}$,

$s_{37} = \{q_2 = \pi/2, q_4 = -5\pi/6\}$, $s_{38} = \{q_2 = -\pi/2, q_4 = -5\pi/6\}$,

$s_{39} = \{q_2 = \pi/2, q_4 = 0\}$, $s_{40} = \{q_2 = 0, q_4 = 0\}$,

$s_{41} = \{q_2 = \pi/2, q_4 = 0\}$, $s_{42} = \{q_3 = -\pi/2, q_4 = 0\}$,

$s_{43} = \{q_3 = \pi/2, q_4 = 0\}$, $s_{44} = \{q_3 = 0, q_4 = 0\}$